RSC Advances

ROYAL SOCIETY
OF **CHEMISTRY**

www.rsc.org/advances

Journal Name

PAPER

A study to initiate development of sustainable Ni/γ-Al₂O₃ catalyst for hydrogen production from steam reforming of bio-mass derived glycerol

Gullapelli Sadanandam, Kasala Ramya, Donthamsetti Bhanu Kishore, Valluri Durgakumari*, Machiraju Subrahmanyam, and Komandur V. R. Chary

Glycerol steam reforming, a potential technology for hydrogen production for fuel cell applications, is of great research interest in recent times. Using aqueous glycerol, a by- product in bio diesel production as direct feed for steam reforming is a promising way to produce hydrogen. Ni (5, 10, 15, 20 and 25 wt %) loaded on commercial γ-Al₂O₃ by impregnation method are used to study steam reforming of ₁₀ glycerol. These catalysts were characterized by XRD, EDAX, BET surface area, TPR, NH₃-TPD, TEM, CHNS and Raman techniques. The catalysts are evaluated time on stream for effect of Ni loading, temperature, and glycerol to water mole ratio (GWMRs). Under the parameters investigated, 15 wt% Ni/γ-Al₂O₃ was found to be the most promising catalyst in terms of glycerol conversion and hydrogen production with minimum coking. The characterization of the catalysts clearly establishes that interaction of Ni^{2+} with γ-Al₂O₃ support; Ni^{2+} reducibility, particle size, and acidity of the support are seen governing the stable activity of the catalysts. Thus a structure activity ₁₅ correlation has been established on Ni/γ-Al₂O₃ catalysts.

1. Introduction

The depletion of global fossil fuel resources, growing environmental impact and energy security concerns, urge us to ₂₀ find new alternative routes for hydrogen production.[1-7] There is tremendous amount of research being pursued towards development of H₂ production technologies for fuel cell applications as fuel cells that consume hydrogen are environmentally clean and highly efficient devices for electrical ₂₅ power generation.[8] The full environmental benefit of generating power from hydrogen fuel cells is achieved when hydrogen is produced from renewable sources like solar power and biomass. In this context, conversion of cheap and available biomass or biomass derived by-products for H₂ production is considered to ₃₀ be a promising approach to meet the requirement of H₂ and to realize sustainable development. To date, glycerol has been considered as an alternative fuel for hydrogen production because it is a by-product of bio diesel production, which uses vegetable oils or fats as feedstock. Hence, in this context, hydrogen ₃₅ production from steam reforming of glycerol seems to be a promising alternative. The reaction that describes the production of hydrogen from glycerol is:

$$C_3H_8O_3 + 3H_2O \longrightarrow 3CO_2 + 7H_2 \qquad (1)$$

The steam reforming of glycerol to produce hydrogen using ₄₀ catalysts has been investigated in the recent decade.[9-17] The steam reforming of glycerol by noble metal catalysts is of high cost and the use of low-cost non noble catalysts would be advantageous from the economical point of view. This reaction is very interesting for its operational characteristics and greater ₄₅ efficiency. Noble metal supported catalysts are more active and less susceptible to carbon deposition than non-noble metals.[11-13] At an industrial scale, the use of Ni supported catalysts for steam reforming is interesting because this catalyst is of low cost and high availability than noble metals. Both development and ₅₀ stability of Ni supported catalysts are subjects of investigation.[14,15] The use of Ni-based catalysts is due to their high efficiency for the cleavage of C-C, O-H, and C-H bonds in hydrocarbons and also they catalyze the water-gas shift reaction removing adsorbed CO from the surface of catalyts.[16] Ce, Mg, Zr, ₅₅ and La modifying Ni/Al₂O₃ enhanced the hydrogen selectivity with minimum coking.[18] More recently, the glycerol steam reforming was evaluated on Ni supported CeO₂, Al₂O₃, and CeO₂-promoted Al₂O₃; the incorporation of low ceria loadings enhanced catalytic activity, while increasing ceria contents ₆₀ reduced the capacity of catalyst to convert intermediate oxygenated hydrocarbons into hydrogen.[19]

Ni/Al₂O₃ catalysts suffer deactivation during the steam reforming of oxygenated hydrocarbons due to the formation of carbonaceous deposits and the sintering of metallic phase. Coke ₆₅ formation is usually related to dehydration, cracking, and polymerization reactions taking place on the acid sites of Al₂O₃,[20] while the sintering of metallic phase can be associated to a transition of Al₂O₃ to crystalline phase during reaction.[21] Using supported catalysts of Rh/ Al₂O₃ and Ni on Al₂O₃, MgO, CeO₂, ₇₀ carbonaceous deposits were formed from olefins produced by the glycerol thermal decomposition and temperatures above 650 °C favoured the generation of encapsulated carbon that decreases the catalyst stability.[22] Using Ni/α-Al₂O₃ and Ni/α- Al₂O₃ modified with ZrO₂ and CeO₂, Ni/α-Al₂O₃ modified CeO₂ catalysts ₇₅ displayed a great stability and its basic character inhibits reactions that form carbonaceous deposits deactivating the catalyst.[23] On Ni loaded Al₂O₃, ZrO₂, and CeO₂ catalysts, used in glycerol reforming the stable activity and maximum H₂ selectivity are observed on Al₂O₃ but coke formation rate is more ₈₀ on Al₂O₃.[24] The effect of Ni precursors on Al₂O₃ catalysts used in glycerol reforming reaction is studied and it is inferred that high Ni dispersion and small Ni particle size promote the catalyst

activity. [25]

Previous thermodynamic studies of glycerol-steam system indicate complete glycerol conversion with high attainment of H_2 yield.[26-30] These studies also suggest that carbon formation is inhibited at high reaction temperature (>900 K), low pressure and high steam-to-glycerol ratio (STGR, 12:1). Adhikari et al considered the thermodynamic equilibrium analysis for glycerol-steam reforming varying parameters, viz. pressure of 1-5 atm, temperature 600-1000 K, and STGR of 1:1-9:1.[29] The best conditions for producing hydrogen are at temperatures higher than 900 K, atmospheric pressure, and a molar ratio of glycerol to water 1:9 as CH_4 production is minimized and carbon formation is thermodynamically inhibited under these conditions.

In our previous work, we have reported the effect of catalyst size in glycerol steam reforming for H_2 production over Ni/SiO_2, where 2x2 & 2x4 mm catalysts promote coke formation at high temperature (600 °C). The higher size 3x5 mm improves the catalytic performance & minimizes coke formation.[31] The present investigation is a part of the ongoing activity on catalyst development for hydrogen production from bio-mass derived glycerol for 2-3 kW PEMFC system to meet the immediate requirement of alternate clean energy based back-up power supply for telecom towers, sponsored by Ministry of New & Renewable Energy (MNRE), Govt of India. There is no commercial catalyst available for glycerol reforming and IICT has initiated catalyst development based on the previous experience on development of methanol reforming.[32] $Ni/\gamma-Al_2O_3$ is a well established system fundamentally as a catalyst for methane reforming and glycerol reforming is altogether a new activity with more number of carbon atoms and high coking rate. The present investigation details the preparation, characterization and time on stream activity of $Ni/\gamma-Al_2O_3$ catalysts and an understanding of the stable and sustainable activity of these catalysts is discussed in terms of acidity, reducibility, Ni crystallite size and coking rate.

2 Materials and methods

2.1 Chemicals

$\gamma-Al_2O_3$ extrudates (Engelhard corporation, AL-3996) with surface area of 192 m^2g^{-1}, Ni $(NO_3)_2.6H_2O$ from Sigma-Aldrich, and Glycerol from Qualigens Fine Chemicals Pvt. Ltd. (India) were used.

2.2 Catalyst Preparation

Nickel (5, 10, 15, 20 and 25 wt %) was loaded on $\gamma-Al_2O_3$ (4x6 mm) by impregnation method. Impregnation methods are generally used on preformed supports for high dispersion and controlled size of active sites. The method involved addition of $\gamma-Al_2O_3$ to a known amount of Ni $(NO_3)_2.6H_2O$ dissolved in distilled water. Excess water was evaporated to dryness under constant stirring with slow heating. The dried sample was calcined at 500 °C/5h in air. The catalysts with 0, 5, 10, 15, 20 and 25 (wt %) of nickel loaded $\gamma-Al_2O_3$ were labelled as A, 5NA, 10 NA, 15NA, 20NA and 25NA. The Ni loaded $\gamma-Al_2O_3$ catalysts were used in glycerol steam reforming at glycerol to water mole ratio (GWMRs) of 1:9 and 650 °C and the used catalysts were labelled as 5NA-1-9, 10NA-1-9, 15NA-1-9, 20NA-1-9 and 25NA-1-9. Nickel loaded $\gamma-Al_2O_3$ catalyst (15 wt %) was used in

glycerol steam reforming at different temperatures (500, 550, 600 and 650 °C using glycerol to water mole ratio 1:9) and different GWMRs (1:3, 1:6 and 1:9 at 650 °C) and were labelled as 15NA-500, 15NA-550, 15NA-600, 15NA-650, 15NA-1-3, 15NA-1-6 and 15NA-1-9 respectively.

2.3 Catalyst Characterization

The X-ray diffraction (XRD) patterns of the $Ni/\gamma-Al_2O_3$ fresh and used catalysts were recorded with Rigaku Miniflex diffractometer with a nickel filtered Cu Kα radiation (λ = 0.15406 nm) from 2θ = 5- 80°, with the beam voltage and beam currents of 40 kV and 100 mA respectively. The crystallite sizes of the catalysts were calculated using Debye-Scherrer equation (Kλ/βcosθ). Elemental analysis was carried out using Link, ISIS-300, Oxford, energy - dispersive analysis of X-ray spectroscopy (EDAX). The BET (Brunauer – Emmett – Teller) surface areas of fresh and used samples were measured by N_2 adsorption at -196 °C in an Autosorb - I (Quantachrome) instrument. Transmission Electron Microscopy (TEM) studies were conducted on TECHNAI 20B2 S-Twin unit operated at 120 kV with a filament current of 28 mA. The carbon contents were estimated using Elementar, Vario Microcube (Germany) CHNS analyser and calibrated with sulphanilic acid using samples in duplicate. The sample was dropped in to the combustion tube automatically and subjected to combustion temperature up to 1200°C. Complete combustion of all samples is ensured with a special oxygen jet injection Tungsten oxide (catalyst for oxidation) The He carrier gas transfers the combustion gaseous products in to the copper tube where nitrogen oxide is reduced to molecular N_2 at 850 °C temperature. The mixature of helium, CO_2, H_2O, SO_2 are guided to specific adsorption traps and measurement. Nitrogen travels to TC detector. Confocal Micro-Raman spectra were recorded at room temperature in the range of 1000-2000 cm^{-1} using a Horiba Jobin-Yvon Lab Ram HR spectrometer with a 17 mW internal He-Ne (Helium-Neon) laser source of excitation with wavelength of 632.8 nm. The catalyst sample in powder form (about 5-10 mg) was usually spread onto a glass slide below the confocal microscope for measurements. Temperature programmed reduction (TPR) was carried out in a quartz micro reactor interfaced to gas chromatography with thermal conductivity detector (GC with TCD) unit. For TPR analysis, the catalyst sample of about 50 mg was loaded in an isothermal zone of a quartz reactor (i.d. = 6 mm, length = 30 cm) heated by an electric furnace at a rate of 10 °C/min to 300 °C in flowing helium gas at a flow rate of 30 ml/min, which facilitates the desorption of physically adsorbed water. Then after the sample was cooled to room temperature, the helium was switched over to 30 ml/min reducing gas of 5% H_2 in argon and the temperature was increased to 1000 °C at a rate of 5 °C/min. Hydrogen consumption was measured by means of thermal conductivity detector. The steam formed during reduction was removed by a molecular sieve trap prior to detection. The acidity of the catalysts was measured by temperature programmed desorption of ammonia (NH_3 -TPD). In a typical experiment, 0.1 g of catalyst was loaded and pretreated in He gas at 300 °C for 2 h. After pretreatment the temperature was brought to 100 °C and the adsorption of NH_3 is carried out by passing a mixture of 10 % NH_3 balance He gas over the catalyst for 1h. The catalyst surface

was flushed with He gas at the same temperature for 2 h to remove the physisorbed NH_3. TPD of NH_3 was carried with a temperature ramp of 10 °C/min and the desorption of ammonia was monitored using thermal conductivity detector (TCD) of a
5 gas chromatograph.

2.4 Catalyst Evaluation

Glycerol steam reforming reactions were carried out using a fixed bed, tubular down flow quartz reactor of 18 mm diameter with a
10 thermocouple of 2 mm width. The reactor was provided with a pre-heater, a syringe pump, a cold condenser and gas flow meter. The catalyst (2g) was loaded in the middle of the reactor. The reactor was placed in a tubular furnace with an inner diameter of 25 mm. The feed mixture (1: 3 to 1:9 mole ratio of glycerol to
15 water) was fed into the vaporizer using a syringe (B.Braun) pump. The feed entering the pre-heater was maintained at 500 ºC before reaching the catalyst bed. A Nippon (NC-2538) temperature controller was used for maintaining the temperature of pre-heating zone and catalyst bed of the reactor. The
20 conversion of glycerol was calculated from the volume of the condensate. The total gas is measured to understand the glycerol to gaseous products and the main products H_2, CO_2, CO and CH_4 are analysed by Gas Chromatography (Shimadzu GC - 2014) using Thermal Conductivity Detector (TCD), Carboxen 1000
25 column and Helium as carrier gas. The other gas products observed in trace quantities are C_2 products. Liquid products like acetaldehyde, acetone, methanol, and acroline were analysed by GC-MS. Carbon deposition is obtained by weighing catalysts at the end of the reaction and compared with carbon from CHNS
30 analysis.

Glycerol conversion and gas composition are calculated as per the following equations:

$$Xgly (\%) = \frac{Gly\ in - Gly\ out}{Gly\ in} \times 100 \quad (2)$$

$$Xgas(\%) = \frac{Xgas(\mu l)}{Total\ gas\ (\mu l)} \times 100 \quad (3)$$

35 Where, Xgly (%) = Glycerol conversion

Xgas (%) = gas (%) where X is H_2, CO_2, CO and CH_4

In all the glycerol steam reforming reactions 6 ml of feed was used. Prior to the reaction, catalysts were reduced using 10 % H_2/N_2 at 550 ºC/5h. The evaluation studies were carried out for
40 25 h time on stream varying parameters.

3 Results and Discussion
3.1 Catalyst Characterization
3.1.1 XRD

45 *Fresh catalysts:* X-Ray diffraction patterns of the catalysts with different loadings of Ni on γ-Al_2O_3 calcined at 500 ºC are shown in Fig.1A. The characteristic peaks of NiO are seen at 2θ of 37.32°, 43.36°, 62.99°, 75.56° and 79.56° corresponding to (111), (200), (220), (311), and (222) planes of NiO (JCPDS # 75-
50 0197).[33] XRD patterns clearly explain that with an increase in Ni loading on γ-Al_2O_3, the NiO crystallite size is increasing and calculated from X-ray line broadening of NiO peak (2θ = 43.36°) using the Scherrer equation and values are shown in Table 1. The

NiO particle size varied from 8.5 nm (10NA) to 13.1 nm (25NA).
55 On the other hand, the diffraction peaks at 2θ = 39.2°, 46.2° and 66.9° confirm presence of γ-Al_2O_3. The characteristic peaks of $NiAl_2O_4$ spinel (2θ° = 37.32°, 46.2°, and 66.9°) are very close to that of NiO and γ-Al_2O_3 and cannot be distinguished.

Used catalysts: Diffraction patterns of different Ni loaded γ-
60 Al_2O_3 catalysts studied for 25 h time on stream at a reaction temperature of 650°C and GWMRs 1:9 are presented in Fig.1B. The XRD of all five catalysts show peaks at 44.38°, 51.72°, and 76.2°and these reflections are assigned to metallic Ni crystallites. Characteristic peaks of γ-Al_2O_3 (2θ = 39.2°, 46.2°, and 66.9°) are
65 also detected in all the catalysts. The XRD patterns of 15NA (15 wt% Ni/γ-Al_2O_3) catalyst evaluated in glycerol reforming at different temperatures are presented in Fig. 2A. The characteristic peaks seen at 44.38°, 51.72°, and 76.2° assigned to metallic Ni crystallites are increasing with temperature and the crystallite size
70 is calculated from X-ray line broadening of Ni peak (2θ = 44.38°) and values are shown in Table 2.[31,33] 15NA catalyst is further studied using different GWMRs at 650 °C for 25 h and the diffraction patterns are shown in Fig. 2B. With an increase in steam ratio, nominal increase in Ni crystalline size is seen. These
75 studies show that the effect of temperature on Ni sintering is more pronounced compared to steam. The reducible NiO phase is observed as metallic Ni peak in the XRD of all used catalysts. No carbon peak is observed in the XRD of all used catalysts as the carbon deposition is below the XRD detection range. The carbon
80 deposition is detected by CHNS and Raman.

3.1.2 EDAX

EDAX analysis of fresh samples was carried out to determine nickel content on γ-Al_2O_3 and the data is shown in Table 1. The
85 composition of the Ni loaded on γ-Al_2O_3 catalysts evaluated in glycerol reforming is shown in Table 2. EDAX analysis of Ni loaded γ-Al_2O_3 used catalysts shows low Ni content compared to calcined catalysts due to carbon deposition. The carbon deposition decreased up to 15NA catalyst and at higher loadings
90 (20NA and 25NA) carbon deposition increased. When 15 NA is studied under different GWMR ratios, the Ni% decreased with decreasing steam. The carbon deposition is also seen increasing with decreasing steam. The observed decrease in Ni content is due to increase in the carbon on surface layers which may change
95 the ratios.

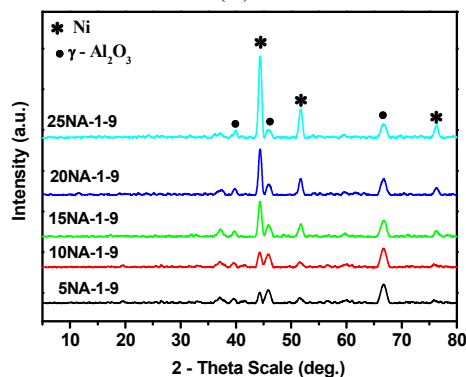**Table. 1** Physical characteristics of Ni/γ-Al_2O_3 calcined catalysts

Catalysts	NiO Crystallite size (nm) from XRD	Ni (wt %) by EDAX	BET surface area (m^2 g^{-1})	[a]H_2 consumption (mmol/g$_{cat}$)/Ni reducibility (%)	[b]Acidity (µmol/g$_{cat}$)
A	--	--	192	--	--
5NA	--	4.9	185	0.55/65	300
10NA	8.5	10.2	179	1.14/67	--
15NA	10.1	16.3	175	1.73/68	160
20NA	12.3	21.1	170	2.41/71	--
25NA	13.1	24.2	162	2.98/70	85

[a]H_2 consumption/ Ni reducibility (%) from TPR analysis
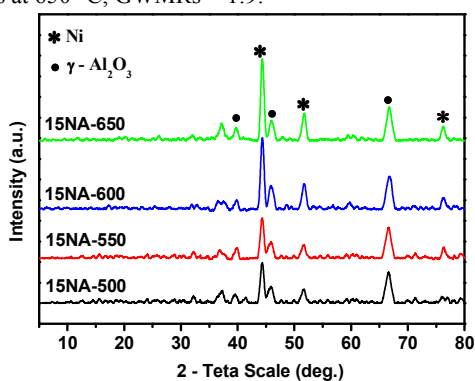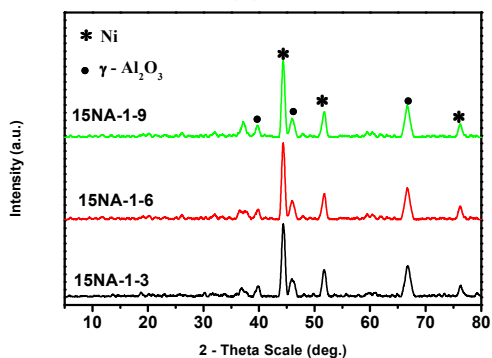[b]Acidity from NH_3-TPD analysis
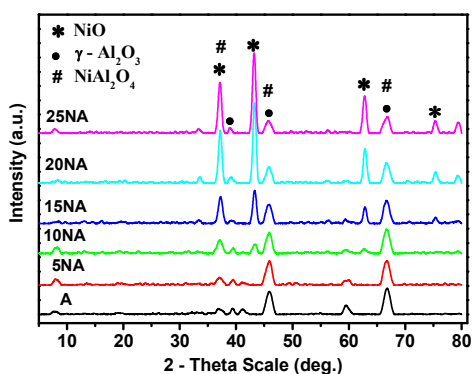
(A)

(B)

Fig. 1 XRD of Ni/γ-Al₂O₃ (A) calcined catalysts (B) used catalysts at 650 °C, GWMRs = 1:9.

(A)

(B)

Fig. 2 XRD of 15NA catalyst used (A) at different temperatures (°C) at 1:9 GWMRs, and (B) different GWMRs at 650 °C.

Table. 2 Physical characteristics of Ni/γ-Al₂O₃ used catalysts

Catalysts	Ni Crystallite size (nm) from XRD	Elemental composition from EDAX		[a]Carbon (%) from CHNS analysis	[b]BET surface area ($m^2 g^{-1}$)
		Ni %	C %		
5NA-1-9	9.5	3.9	2.5	4.2	165
10NA-1-9	9.8	8.4	2.0	3.8	150
15NA-1-9	10.6	14.1	1.5	3.1	150
20NA-1-9	13.1	18.6	2.5	4.8	140
25NA-1-9	14.9	21.5	3.5	5.9	125
15NA-1-6	10.4	12.3	3.0	7.6	135
15NA-1-3	10.1	11.2	3.8	9.7	120
15NA-600	10.5	13.8	1.6	3.2	--
15NA-550	10.3	13.4	1.8	3.4	--
15NA-500	10.1	13.0	2.0	3.7	--

[a]Standard deviation of Carbon = ± 0.1%

[b]Standard deviation of BET surface area = ± 5

3.1.3 BET Surface area

The surface area of γ-Al₂O₃ and Ni/γ-Al₂O₃ fresh and used catalysts obtained are shown in Table 1 and 2. The surface area of γ-Al₂O₃ is around 192 m^2g^{-1} and this decreased with increase in Ni loading.[34] The surface area of the used catalysts also decreased, which may be seen as due to some factors like reaction temperature and carbon deposition. The alumina structure undergoing transition at higher temperature may reduce the surface area. However in the interacted aluminas, transitions are slow and the corresponding textural changes are not observed in XRD. The coke deposited on the surface of catalyst may block the pores and results in decreased surface areas. [31, 35]

3.1.4 CHNS Analysis

CHNS analysis was carried out to understand the amount of carbon deposition studied under different reaction conditions and the data is shown in Table 2. Carbon deposition is more at lower loadings of Ni (5NA and 10NA) due to acid sites available on γ-Al₂O₃ surface (Table 1). With increasing Ni content the acid sites decreased and less coking is observed on 15NA. However with further increase in nickel, coking rate increased. Of all the catalysts studied, the carbon deposition observed is low on15NA catalyst. 15NA catalyst studied further at different temperature and GWMRs showed more carbon deposition at low temperature and low steam.[36] The reasons are discussed in catalyst evaluation section.

3.1.5 TPR

TPR analyses were performed to investigate the reducibility of Ni^{2+} species present in the calcined catalysts and the results are shown in Fig. 3 and Table 1. TPR profiles of different Ni loaded γ-Al₂O₃ catalysts show two distinct reduction processes. A less intense peak seen between 300 and 350 °C is due to the reduction of Ni^{2+} species that are in weak interaction with support. A broad high temperature peak in the region of 450 -800 °C with T_{max}

of reduction around 650°C that may be seen due to strong interaction Ni^{2+} with γ-Al_2O_3 support.[37, 38] At higher Ni loadings (20NA and 25NA) broad signal is shifted to a lower temperature (550 °C), indicating presence of Ni^{2+} species with decreased strength of interaction. This indicates that at higher Ni loadings, the support is with heterogeneous distribution of Ni^{2+} species. The reduction peak appearing at higher temperatures may be attributed to the reduction of Ni^{2+} ions from non-stoichiometric nickel aluminate species.[16, 38]
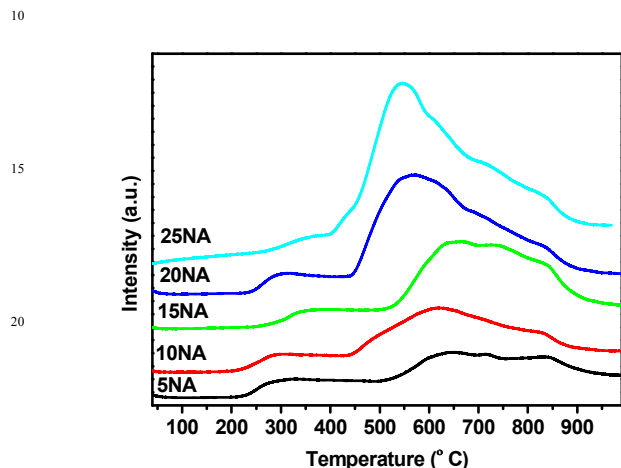

Fig. 3 TPR analysis of Ni loaded γ-Al_2O_3 catalysts.

3.1.6. NH₃-TPD

Ammonia adsorption–desorption technique usually enables one to determine the strength of acid sites present on the surface of catalyst. The TPD of NH_3 profiles of typical Ni/γ-Al_2O_3 catalysts (5NA, 15NA and 25NA) are shown in Fig. 4. Total acidity (300 - 700°C) on these decreased with an increase in Ni loading (Table 1).[20]
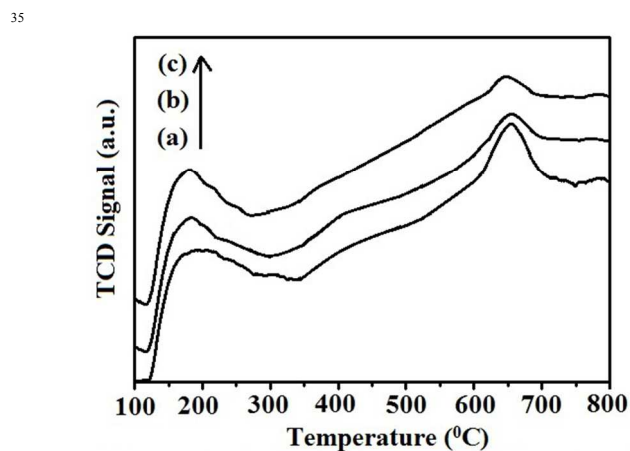

Fig. 4 NH₃-TPD analysis of Ni/γ-Al_2O_3 catalysts (a) 5NA, (b) 15NA and (c) 25NA

3.1.7 TEM

The morphology of deposited carbon is studied by TEM and photographs of representative samples are shown in Fig.5. On 15NA-1-9 sample (Fig.5 a & b) Ni metal particles are observed as dark spots on the surface of γ-Al_2O_3 support. At higher Ni loadings, i.e on 20NA-1-9 and 25NA-1-9 TEM images show formation of more carbon filaments with dispersed nickel particles (Fig.5 c & d). The glycerol steam reforming reaction over Ni/γ-Al_2O_3 catalyst leads to the formation of graphitic flake-like carbon (filamentous carbon or carbon nano tubes) and amorphous carbon and the results obtained are in confirmation with the reported literature.[39-41]
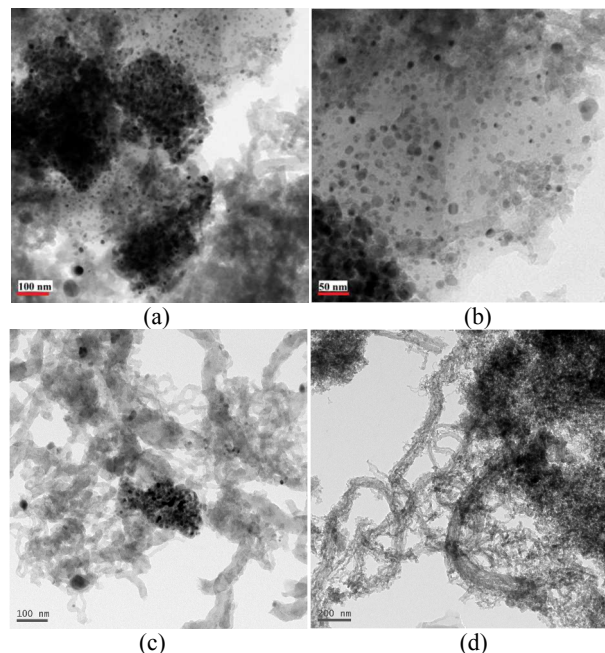

Fig. 5 TEM images of used Ni/ γ-Al_2O_3 catalysts (a) & (b) 15NA-1-9, (c) 20NA-1-9, and (d) 25NA-1-9.

3.1.8 Raman spectra

Raman spectroscopy is used to characterize post-reaction catalysts because it is a powerful technique for characterizing the structure of carbonaceous materials. On all catalysts Raman spectra revealed two broad bands around 1335 cm^{-1} (D band) and 1591cm^{-1} (G band) (Fig. 6). The former is ascribed to the disordered carbon (amorphous) and the latter is attributed to in-plane carbon–carbon stretching vibrations (E_{2g}) of the graphitic carbon.[39,40,43] In all cases the D band is more intense than the G band, indicating a predominance of disordered carbon. The degree of graphitic carbon deposits can be estimated by the ratio of the area of the D band to that of the G band (I_D/I_G); a higher degree of graphitization produces a lower I_D/I_G ratio. The results indicate that on 15NA disordered carbon and graphitic carbon are minimum as shown in Fig. 6a. The 15NA catalysts are further studied at different GWMRs and the used catalysts are subjected to Raman spectra as (Fig. 6b). These spectra clearly explain that by decreasing steam, the formation of both types of carbon is seen inccreasing.[4]
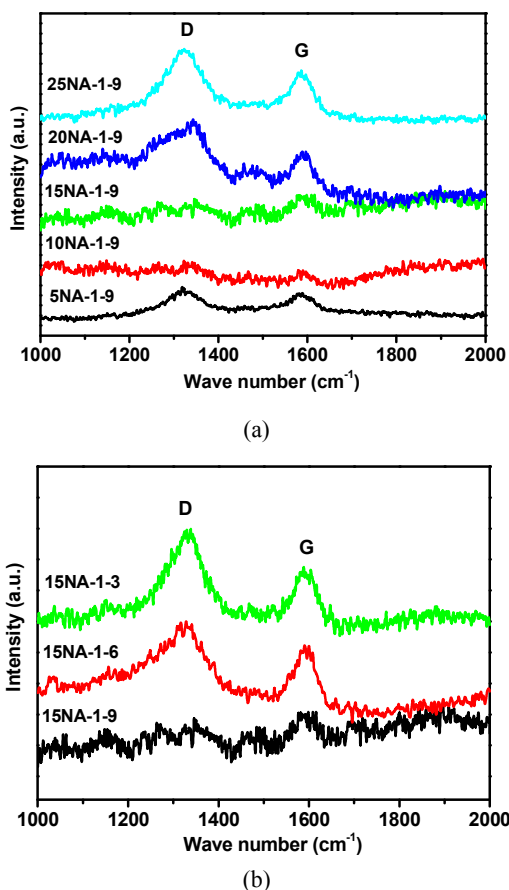
(a)

(b)

Fig. 6 Raman spectra of used Ni/ γ-Al$_2$O$_3$ catalysts (a) different Ni loading at 1:9 GWMRs and 650 °C, (b) 15NA catalyst at different GWMRs and 650 °C.

3.2 Catalyst Evaluation

3.2.1 Effect of Ni loading on γ-Al$_2$O$_3$

Glycerol steam reforming reaction on Ni/γ-Al$_2$O$_3$ catalysts is studied at 1:9 GWMRs and 650 °C and the results are shown in Fig. 7. The glycerol conversion and H$_2$ production rates on 5NA and 10NA catalysts decrease with time on stream.[44] On 15NA catalyst steady glycerol conversion activity is observed for 25 h. 100% glycerol conversion and 67.5 % of H$_2$ in the gas stream with minimum coking are achieved on this catalyst. At higher Ni loadings (20NA and 25NA) also steady conversion is observed for 15h, after which the conversion as well as H$_2$ production rate are showing decreased tendency. On 5NA and 10NA catalysts, activity decreased with time on stream that may be seen as due to the acid sites of alumina available on these catalysts forming coke with time and deactivating the catalyst.[20,25] At a given metal loading, the number of active sites in a catalyst is a function of the metal dispersion. The surface saturation of Ni over γ-Al$_2$O$_3$ may be seen around 15% of Ni. The Ni particle formed at this coverage appears to be more suitable for stable activity in glycerol reforming. Above15% Ni loading though there is no much difference observed in the particle size of Ni, the TPR clearly shows that the Ni particle formed at higher loading (20NA and 25NA) is reduced relatively at low temperature compared to 15NA. This shows that particle obtained on 15NA is out Ni-O-Al linkage. Above this loading the possibility of formation of free NiO is seen, that may accelerate the Ni particle

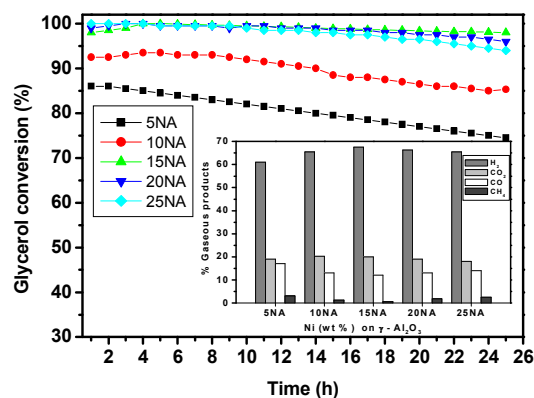size affecting the stable activity.[45] Thus 15NA, catalyst is further studied.

Fig. 7 Effect of Ni (wt %) on γ-Al$_2$O$_3$ catalysts in glycerol reforming at 1:9 GWMRs and 650°C. Inset: product gas distribution.
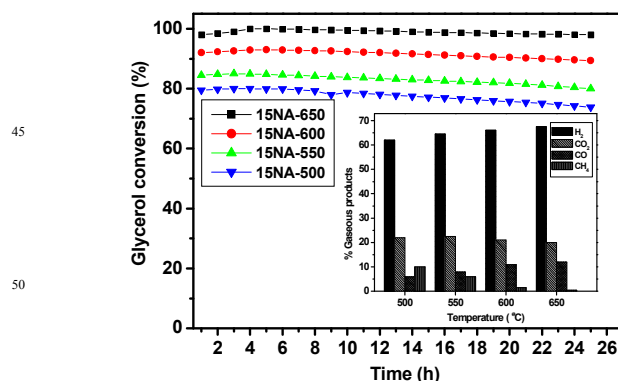

Fig. 8 Effect of Temperature on 15NA in glycerol steam reforming; GWMRs = 1:9, Inset: product gas distribution.

3.2.2 Effect of Temperature

Glycerol conversion and product gas distribution on 15NA are shown as a function of temperature in Fig. 8. The results show that at 500-600 ºC, activity is seen decreasing slightly with time. Below 600 ºC due to dehydrogenation and dehydration, the formation by products results and the side reactions of these by products may deposit carbon with time. This is possibly minimised at higher temperatures due to complete decomposition of glycerol to CO and H$_2$. Fig. 8 (Inset) clearly explains the product gas distributions on 15NA as a function of temperature at 1:9 GWMRs. With increasing temperature from 500 to 650 °C, the glycerol conversion and hydrogen percentages are increased due to the endothermic nature of glycerol steam reforming.[19, 44] with increase temperature CH$_4$ is decreased and CO is increased due to methane steam reforming is favoured at high temperature.[25] Fig. 9 clearly explains the glycerol conversion and gas product distribution with time on stream on 15NA catalyst. No change in glycerol conversion is observed for 25h. However decrease in H$_2$ production say 1-2%, decrease in CO$_2$ up to 3% and increases in CO up to 6% are observed. The above results explain that water gas shift reaction decreased with time and

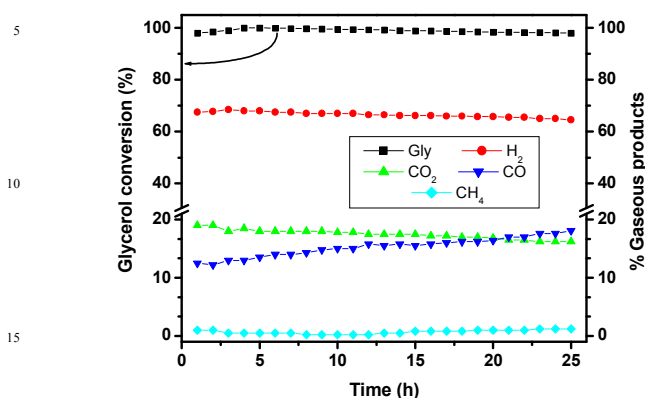building CO concentrations. This may be seen as loss of active sites due to coking with time.[25, 40, 46]

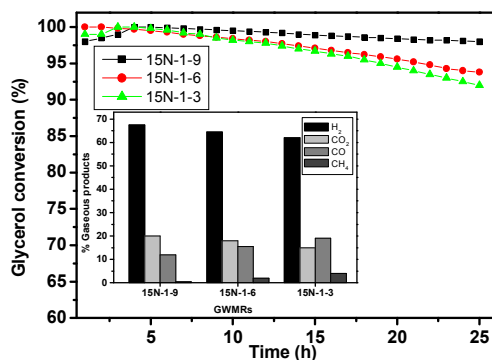**Fig. 9** Time on steam activity on 15NA catalyst is using in glycerol steam reforming at 1:9 GWMRs and 650°C.

Fig. 10 Effect of GWMRs on 15NA catalyst in glycerol steam reforming at 650 $^{\circ}$C, Inset is gaseous product distribution.

3.2.3 Effect of GWMRs

Analysing the effect of reaction temperature on the catalytic performance of 15NA, the temperature of 650 $^{\circ}$C was chosen to study the effect of GWMRs. Additionally steam reforming is an energy-intensive process and GWMRs optimization is necessary to minimize the process cost. Glycerol content in the feed was changed and the results are depicted in Fig.10. As the GWMRs increased (steam decreased), the glycerol conversion decreased with time due to carbon deposition. The gaseous product distribution also changes, wherein the products H_2 and CO_2 are decreased and CO and CH_4 are increased due to the absence of water gas shift reaction and methane steam reforming.[25, 33,44]

3.2.4 Coke formation

Coke formation during steam reforming causes rapid deactivation of catalysts and thereby results in low durability. Therefore, it is interesting to determine the reaction conditions to minimize coke formation for the design of efficient carbon resistant catalysts. Fig.11 represents the carbon formation as a function of Ni loading and GWMRs in glycerol steam reforming. The carbon deposition is calculated with the formula:

$$C_{deposition} \text{ (mg g}^{-1} \text{ cat. h}^{-1}) = (M_T - M_{cat}) / (M_{cat} \text{ x T})$$

Where M_T is the total mass of the catalyst and carbon produced after 25h of reaction, M_{cat} is the mass of the catalyst before reaction, and T is total reaction time (25h). With an increase Ni on γ-Al$_2$O$_3$, the carbon formation decreases (1.9 to 1.3 mg carbon g^{-1} cat. h^{-1}) up to 15% Ni and beyond, carbon formation increased to 3.3 mg carbon g^{-1} cat. h^{-1}. 5NA and 10NA show more carbon indicating the availability of acid sites on alumina support responsible for coking. Coking is less on 15NA indicating that the Ni crystallite formed at this concentration is more suitable for reforming (optimum dispersion). Above this loading, on 20NA and 25NA coking increased due to increase in Ni crystallite size. 15NA catalyst further studied at different GWMRs (Fig. 11 inset) is evaluated for carbon deposition. The carbon formation increased with decreasing steam (1.3- 4.3 mg carbon g^{-1} cat. h^{-1}).
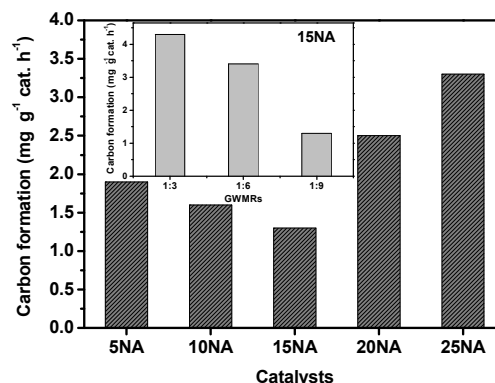

Fig. 11 Effect of Ni loading on γ-Al$_2$O$_3$ on the comparison of carbon formation at 650 $^{\circ}$C and GWMRs = 1:9, Inset is carbon formation in different GWMRs on 15NA catalyst at 650°C temperature.

4 Conclusions

Ni/γ-Al$_2$O$_3$ catalysts prepared by impregnation method were evaluated for H_2 production in glycerol steam reforming. The 15 wt% Ni/γ-Al$_2$O$_3$ catalyst produced maximum H_2 production and minimum coking with 100% glycerol conversion at 650 $^{\circ}$C and 1:9 GWMRs. XRD and TPR results are indicating that Ni^{2+} is strongly interacted with γ-Al$_2$O$_3$ at low loadings. With increasing Ni loading the Ni crystallite size increased and interaction with the support decreased. TPD of NH$_3$ shows that total acidity of γ-Al$_2$O$_3$ support decreased with Ni loading. Raman studies of used catalysts also indicate that surface acidity at lower loadings and Ni crystallite size at higher loadings are responsible for coking. The evaluation and characterization of Ni/γ-Al$_2$O$_3$ catalysts clearly establish that Ni^{2+} in strong interaction with γ-Al$_2$O$_3$ support resulted in well dispersed Ni active sites that are responsible for stable and sustainable activity with minimum coking.

Notes and References

* Corresponding author E-mail: durgakumari@iict.res.in
Tel: +91-40-27193165, Fax: +91-40-27160921
5 Inorganic and Physical Chemistry Division, Indian Institute of Chemical Technology, Hyderabad-500 607, India

1 C. H. Zhou, J. N. Beltramini, Y. X. Fan and G .Q. Lu, *Chem. Soc. Rev.,* 2008, **37**, 527-549.

10 2 J.N. Chheda, G.W. Huber and J.A. Dumesic, *Angew Chem. Int Ed.,* 2007, **46**, 7164-7183.

3 G. D. Wen, Y. P. Xu, H. J. Ma, Z. S. Xu and Z. J. Tian, *Int. J. Hydrogen Energy* 2008, **33**, 6657-6666.

4 C. Wu, Z. Wang, P. T. Williams and J. Huang, *Sci. Rep.,* 2013, 15 **3**, 2742; DOI:10.1038/ srep02742.

5 G. Sadanandam, K. Lalitha, V. Durga Kumari, M.V. Shankar and M. Subhramanyam, *Int. J. Hydrogen Energy,* 2013, **38**, 9655- 9664

6 I. Fechete, Y. Wang, J. C. Vedrine, *Catal. Today*, 2012, **189**, 20 2-27.

7 H. Ziaei-azad, C.X. Yin, J. Shen, Y. Hu and D. Karpuzov, *J. catal.,* 2013, **300,** 113-124.

8 R.R. Davda, J.W. Shabaker, G.W. Huber, R.D. Cortright and J.A. Dumesic, *Appl. Catal., B,* 2005, **56**, 171-186.

25 9 P. D. Vaidya and A. E Rodrigues, *Chem. Eng. Technol.,* 2009, **32**, 1463-1469.

10 Z. Wei, J. Sun, Y. Li, A. K. Datye and Y. Wang, *Chem. Soc. Rev.,* 2012, **41,** 7994-8008.

11 L. P. R. Profeti, E. A. Ticianelli and E. M. Assaf, *Int. J.* 30 *Hydrogen Energy,* 2009, **34**, 5049-5060.

12 N.J. Luo, J.A. Wang, T.C. Xiao, F.H. Cao and D.Y. Fang, *Catal. Today*, 2011, **166**,123-128.

13 F. Pompeo, G. Santori and N. Nichio, *Int. J. Hydrogen Energy,* 2010, **35**, 8912-8920.

35 14 T. Hirai, N. Ikenaga, T. Miyake and T. Suzuki, *Energy Fuels*, 2005, **19**, 1761-1762.

15 G.W. Huber, J.W. Shabaker and J.A. Dumesic, *Science,* 2003, **300,** 2075-2077.

16 A. Iriondo, V.L. Barrio, J.F. Cambra, P.L. Arias, M.B. 40 Guemez and M. C. Sanchez-Sanchez, *Int. J. Hydrogen Energy,* 2010, **35,** 11622-11633.

17 A. M. D. Douette, S. Q. Turn, W. Wang and V.I. Keffer, *Energy Fuels,* 2007, **21**, 3499-3504.

18 A. Iriondo, V. L. Barrio, J. F. Cambra, P. L. Arias, M. B. 45 Guemez, R. M. Navarro, M. C. Sanchez-Sanchez, and J. L. G. Fierro, *Top. Catal.,* 2008, **49**, 46-58.

19 S. Adhikari, S. Fernando and A. Haryanto, *Catal. Today,* 2007,**129**, 355-364.

20 S. Li, C. Zhang, P. Zhang, G. Wu, X. Ma and J. Gong, Phys. 50 Chem. Chem. Phys., 2012, **14**, 4066-4069

21 J. G. Seo, M. H. Youn, S. Park, J. S. Chung and I. K. Song, *Int. J. Hydrogen Energy,* 2009, **34,** 3755-3763.

22 V. Chiodo, S. Freni, A. Galvagno, N. Mondello and F. Frusteri, *Appl. Catal., A,* 2010, **381,** 1-7.

55 23 I. N. Buffoni, F. Pompeo, G. F. Santori and N. N. Nichio, *Catal. Commun.,* 2009, **10**, 1656-1660.

24 R. L. Manfro, N. F. P. Ribeiro, and M. M. V. M. Souza, *Catal. Sustainable Energy*, 2012, 60-70, DOI: 10.2478/cse-

2013-0001.

60 25 G. Wu, C. Zhang, S. Li, Z. Han, T. Wang, X. Ma and J. Gong, *ACS Sustainable Chem. Eng*., 2013, **1**, 1052-1062.

26 X. Wang, S. Li, H. Wang, B. Lu and X. Ma, *Energy Fuels*, 2008, **22**, 4285-4291.

27 N. Luo, X. Zhao, F. Cao, T. Xiao and D. Fang, *Energy Fuels,* 65 2007, **21**, 3505-3512.

28 M. L. Dieuzeide and N. Amadeo, *Chem. Eng. Tech*., 2010, **33**, 89-96.

29 S. Adhikari, S. Fernando, S. R. Gwaltney, S. D. Filip To, R. Mark Bricka, and P. H. Steele, *Int. J. Hydrogen Energy*, 70 2007, **32**, 2875-2880.

30 C. C. R. S. Rossi, C. G. Alonso, O. A. C. Antunes, R. Guirardello and L. Cardozo-Filho, *Int. J. Hydrogen Energy*, 2009, **34**, 323-332.

31 G. Sadanandam, N. Sreelatha, M. V. Phanikrishna Sharma, S. 75 Kishta Reddy, B. Srinivas, K. Venkateswarlu, T. Krishnudu, M. Subrahmanyam, and V. Durga Kumari, *ISRN Chem. Eng,* 2012,**2012**, 1-10. http://dx.doi.org/10.5402/2012/591587.

32 V. Durga Kumari, M. Subrahmanyam, A. Ratnamala, D. Venugopal, B. Srinivas, M. V. Phanikrishna Sharma, S.S. 80 Madhavendra, B. Bikshapathi, K. Venkateswarlu, T. Krishnudu, K.B.S. Prasad and K.V. Raghavan, *Catal Commun.*, 2002, **3**, 417-424.

33 K. Kamonsuangkasem, S. Therdthianwong, A. Therdthianwong, *Fuel. Process. Technol*., 2013, **106**, 695- 85 703.

34 E. Salehi, F. S. Azad, T. Harding and J. Abedi, *Fuel. Process. Technol.,* 2011, **92**, 2203-2210

35 C. Wang, B. Dou, H. Chen, Y. Song, Y. Xu, X. Du, L. Zhang, T. Luo and C. Tan, *Int. J. Hydrogen Energy*, 2013, **38,** 90 3562-3571.

36 C. Wang, B. Dou, H. Chen, Y. Song, Y. Xu, X. Du, T. Luo and C. Tan, Chem. Eng. J., 2013, **220**, 133-142

37 M. L. Dieuzeide, V. Iannibelli, M. Jobbagy and N. Amadeo, *Int J Hydrogen Energy*, 2012, **37**, 14926-14930.

95 38 A. Iriondo, J. F. Cambra, M. B. Guemez, V. L. Barrio, J. Requies, M. C. Sanchez-Sanchez and R.M. Navarro*, Int. J. Hydrogen Energy*, 2012, **37**, 7084-7093.

39 D. Z. Mezalira, L. D. Probst, S. Pronier, Y. Batonneau and C. Batiot-Dupeyrat, *J. Mol. Catal., A,* 2011, **340**, 15-23.

100 40 I. Rossetti, A. Gallo, V. D. Santo, C.L. Bianchi, V. Nichele, M. Signoretto, E. Finocchio, G. Ramis, and A. D Michele, *Chem Cat Chem* 2013, **5**, 294 - 306

41 S.P. Chai, S.H.S. Zein, A.R. Mohamed, National Postgraduate Colloquim, School of Chemical Engineering 105 University of Sains Malaysia, Seri Ampangan, 2004, 60-69.

42 A. E. Galetti, M. F. Gomez, L. A. Arrua and M. C. Abello, *Appl. Catal., A,* 2008, **348**, 94-102.

43 M. E. Doukkali, A. Iriondo, P. L. Arias, J. F. Cambra, I. Gandarias and V. L. Barrio, *Int. J. Hydrogen Energy*, 2012, 110 **37,** 8298-8309.

44 V. Dhanala, S. K. Maity and D. Shee, RSC Adv., 2013, **3**, 24521-24529

45 S. Narayanan, and K. Uma, *J. Chem. Soc. Faraday Trans. I.,* 1985, **81**, 2133-2144.

115 46 E. A. Sanchez, and R. A. Comelli, *Int. J. Hydrogen Energy*, 2012, **37,** 14740-14746

Graphical Abstract